Hindawi
Stem Cells International
Volume 2018, Article ID 3272098, 16 pages
https://doi.org/10.1155/2018/3272098

Research Article

The Effects of Platelet-Derived Growth Factor-BB on Bone Marrow Stromal Cell-Mediated Vascularized Bone Regeneration

Maolin Zhang,[1,2,3] **Wenwen Yu**,[4] **Kunimichi Niibe**,[3] **Wenjie Zhang**,[1,2] **Hiroshi Egusa**,[3] **Tingting Tang**,[5] **and Xinquan Jiang**[1,2]

[1]*Department of Prosthodontics, Ninth People's Hospital affiliated to Shanghai Jiao Tong University, School of Medicine, 639 Zhizaoju Road, Shanghai 200011, China*
[2]*Shanghai Key Laboratory of Stomatology & Shanghai Research Institute of Stomatology, National Clinical Research Center of Stomatology, 639 Zhizaoju Road, Shanghai 200011, China*
[3]*Division of Molecular and Regenerative Prosthodontics, Tohoku University Graduate School of Dentistry, 4-1 Seiryo-machi, Aoba-ku, Sendai, Miyagi 980-8575, Japan*
[4]*Department of Oral and Craniomaxillofacial Science & Sleep-disordered Breathing Center, Ninth People's Hospital affiliated to Shanghai Jiao Tong University, School of Medicine, 639 Zhizaoju Road, Shanghai, China*
[5]*Shanghai Key Laboratory of Orthopaedic Implants, Department of Orthopaedic Surgery, Shanghai Ninth People's Hospital, Shanghai Jiaotong University, School of Medicine, Shanghai 200011, China*

Correspondence should be addressed to Xinquan Jiang; xinquanj@aliyun.com

Received 18 March 2018; Revised 9 August 2018; Accepted 16 August 2018; Published 31 October 2018

Academic Editor: Heng Zhu

Regenerative medicine for bone tissue mainly depends on efficient recruitment of endogenous or transplanted stem cells to guide bone regeneration. Platelet-derived growth factor (PDGF) is a functional factor that has been widely used in tissue regeneration and repair. However, the short half-life of PDGF limits its efficacy, and the mechanism by which PDGF regulates stem cell-based bone regeneration still needs to be elucidated. In this study, we established genetically modified PDGF-B-overexpressing bone marrow stromal cells (BMSCs) using a lentiviral vector and then explored the mechanism by which PDGF-BB regulates BMSC-based vascularized bone regeneration. Our results demonstrated that PDGF-BB increased osteogenic differentiation but inhibited adipogenic differentiation of BMSCs via the extracellular signal-related kinase 1/2 (ERK1/2) signaling pathway. In addition, secreted PDGF-BB significantly enhanced human umbilical vein endothelial cell (HUVEC) migration and angiogenesis via the phosphatidylinositol 3 kinase (PI3K)/AKT and ERK1/2 signaling pathways. We evaluated the effect of PDGF-B-modified BMSCs on bone regeneration using a critical-sized rat calvarial defect model. Radiography, micro-CT, and histological analyses revealed that PDGF-BB overexpression improved BMSC-mediated angiogenesis and osteogenesis during bone regeneration. These results suggest that PDGF-BB facilitates BMSC-based bone regeneration by enhancing the osteogenic and angiogenic abilities of BMSCs.

1. Introduction

Reconstruction of bony defects caused by infection, trauma, or tumor resection is still a substantial clinical challenge. Bone marrow stromal cells (BMSCs) possessing regenerative potential have been considered an ideal cell source for bone regeneration [1, 2]. In addition, the combination of BMSCs with particular growth factors, such as bone morphogenetic proteins (BMPs) and vascular endothelial growth factor (VEGF), has been considered a promising strategy for bone tissue regeneration [3].

Platelet-derived growth factor (PDGF), a two-chain polypeptide, was originally identified in platelets [4, 5], and there are five polypeptide isoforms: PDGF-AA, PDGF-AB, PDGF-BB, PDGF-CC, and PDGF-DD [5, 6]. Among these isoforms, PDGF-BB is a unique ligand that can interact with all three PDGF receptors, namely, PDGFR-$\alpha\alpha$, PDGFR-$\alpha\beta$, and PDGFR-$\beta\beta$ [4]. PDGF-BB is a potent mitogen [7, 8] and

chemoattractant for many cell types [9, 10] and has the ability to promote angiogenesis [11]. Thus, PDGF-BB is considered a key regulatory factor in tissue repair and regeneration [12]. Previous studies have demonstrated that PDGF-BB can enhance stem cell-based bone regeneration [13, 14]. However, the mechanisms by which PDGF-BB contributes to stem cell-based bone regeneration still need to be further elucidated. In addition, the short half-life of PDGF within the blood (only a few minutes) limits its efficacy [15]. Therefore, sustained local delivery of PDGF-BB is likely important to achieve ideal results. Forced expression of PDGF-BB by lentiviral transduction may be a useful method to investigate the effects of PDGF-BB on the regulation of stem cell-based bone regeneration. In this system, lentiviral transduction would enable stable and efficient expression of the transgene in cells even after several passages, which can facilitate both *in vitro* and *in vivo* investigations of the mechanism underlying PDGF-BB regulation of stem cell-based bone regeneration.

In this study, we established a PDGF-B-modified BMSC line using a lentivirus gene delivery vector and then explored the mechanism by which PDGF-BB regulates BMSC osteogenic and adipogenic differentiation. We further investigated the mechanism of PDGF-BB-induced vascular endothelial cell migration and angiogenesis. Finally, PDGF-B-modified BMSCs were mixed with a porous calcium phosphate cement (CPC) scaffold and transplanted into a rat critical-sized calvarial defect. Bone regeneration was evaluated using micro-CT and histological analysis.

2. Materials and Methods

2.1. Isolation and Culture of Rat BMSCs. BMSCs were isolated from 4-week-old Fisher 344 rats as previously described [16–18]. Briefly, bone marrow in bilateral rat tibias and femurs was flushed out using Dulbecco's modified Eagle's medium (DMEM, Gibco BRL, Grand Island, NY) containing 10% fetal bovine serum (FBS, Gibco, USA) and antibiotics (penicillin 100 U/mL, streptomycin 100 U/mL), and then, the cells were cultured in DMEM at 37°C in a humidified 5% CO_2 incubator. After two days, the nonadherent cells were discarded. Cells at passages 2 and 3 were used for this study.

2.2. Lentiviral Vector Construction and Transduction. Lentiviral vectors containing the human PDGF-B gene and enhanced green fluorescent protein (eGFP, Lenti-PDGF) or LacZ and eGFP (Lenti-LacZ) were constructed by Cyagen Biosciences, Inc. (Guangzhou, China). Briefly, the target plasmids pLV.EX3d.P/puro-EF1A > PDGFB > IRES/eGFP and pLV.EX3d.P/puro-EF1A > Lacz > IRES/eGFP were constructed using Gateway technology (pLV.EX3d.P/puro-EF1A > Lacz > IRES/eGFP was used as the control), and then, 293FT cells were transfected with the target plasmid together with the helper plasmid (pLV/helper-SL3, pLV/helper-SL4, and pLV/helper-SL5) using Lipofectamine 2000 (Invitrogen) according to the manufacturer's instructions [19]. The supernatant containing the lentivirus particles was harvested and ultracentrifuged. For transduction, BMSCs were cultured for 24 h to reach 70–80% confluence and then transduced with Lenti-PDGF or Lenti-LacZ at a multiplicity of infection of 20. The transduction efficiency was analyzed by flow cytometry to calculate the percentage of eGFP-expressing cells at day 3.

The expression of PDGF-BB in BMSCs was evaluated using real-time reverse transcription polymerase chain reaction (real-time RT-PCR) and Western blotting. The amount of PDGF-BB secreted by PDGF-B-modified BMSCs in the culture medium from each group was detected using a PDGF-BB ELISA kit (Abcam) according to the manufacturer's instructions [19]. All experiments were performed in triplicate.

2.3. Osteogenic Induction of BMSCs. For osteogenic differentiation, cells were seeded in 12-well plates and cultured in osteogenic medium (DMEM, 10% FBS, 1% penicillin/streptomycin, 50 μg/mL L-ascorbic acid, 10 mM glycerophosphate, and 100 nM dexamethasone) with or without PD98059 (10 μM), an extracellular signal-related kinase (ERK) inhibitor (Cell Signaling Technology, Inc.). The osteogenic medium was changed every two days. The expression of osteogenesis-related genes was determined after 3 or 7 days of culture using real-time PCR and Western blotting. Osteogenic differentiation was also evaluated via alkaline phosphatase (ALP) and Alizarin Red S (ARS) staining for calcium deposition. For ALP analysis, cells in each group were fixed with 4% paraformaldehyde on day 7 and then stained with an ALP kit (Beyotime, China). Semiquantitative analysis of ALP activity was performed by testing optical density (OD) values at 405 nm using p-nitrophenyl phosphate (pNPP, Sigma) as the substrate [20]. For ARS analysis, cells from each group were fixed with 95% alcohol for 10 min and then stained with 0.1% ARS solution (Sigma) for 30 min on day 21. For a further quantitative assay, the ARS staining was desorbed with 10% cetylpyridinium chloride (Sigma), and the OD values were determined at 590 nm. The total protein content in each group was measured using a Bio-Rad protein assay kit (Bio-Rad, USA), and ALP and ARS levels were calculated as optical density per microgram of protein. All experiments were performed in triplicate.

2.4. Adipogenic Induction of BMSCs. For adipogenic differentiation, cells in each group were seeded on 12-well plates, cultured in DMEM until they reached 100% confluence, and then cultured in adipogenic medium containing 0.5 mM isobutylmethylxanthine (Sigma), 0.5 mM hydrocortisone, and 60 mM indomethacin (Sigma) with or without PD98059 (10 μM). Intracellular lipid accumulation was stained with Oil Red O as previously described [21]. Briefly, the cells were fixed with 4% paraformaldehyde for 15 min and stained with diluted Oil Red O solution for 10 min. All samples were viewed with an inverted phase contrast microscope (Leica, Germany), and the stained fields were evaluated using Image pro 5.0 (Media Cybernetics, USA). The expression of peroxisome proliferator-activated receptor γ2 (PPARγ2) was analyzed via real-time RT-PCR and Western blotting. All experiments were performed in triplicate.

Table 1: Nucleotide sequences for real-time RT-PCR primers.

Gene	Primer sequence (5′-3′) (forward/reverse)	Product size (bp)	Accession number
PPAR-γ2	TGCAGGTGATCAAGAAGACG TGGAAGAAGGGAAATGTTGG	177	NM_013124
PDGF-BB	CTGCGACCTGTCCAGGTGAG GCACCGTCCGAATGGTCACC	199	NM_033016.2
OPN	CCAAGCGTGGAAACACACAGCC GGCTTTGGAACTCGCCTGACTG	165	NM_012881
OCN	GCCCTGACTGCATTCTGCCTCT TCACCACCTTACTGCCCTCCTG	103	NM_013414
COL-I	CTGCCCAGAAGAATATGTATCACC GAAGCAAAGTTTCCTCCAAGACC	198	NM_053304
GAPDH	GGCAAGTTCAACGGCACAGT GCCAGTAGACTCCACGACAT	76	NM_017008.3

2.5. Real-Time RT-PCR Analysis. Total RNA was extracted from cells using Trizol Reagent (Invitrogen). The total RNA concentration was measured with a Thermo Scientific NanoDrop™ 1000 ultraviolet-visible spectrophotometer (NanoDrop Technologies, Wilmington, DE) as previously described [22]. cDNA was synthesized according to the manufacturer's instructions using a Prime-Script™ RT reagent kit (Takara Bio, Shiga, Japan). Osteogenesis-related marker genes, including *type I collagen (Col-I)*, *osteopontin (OPN)*, and *osteocalcin (OCN)*, and the adipogenic marker gene *PPARγ2* were examined. *Glyceraldehyde-3-phosphate dehydrogenase (GAPDH)* was used as the housekeeping gene for normalization of RNA expression levels. All experiments were performed in triplicate. The PCR primer sequences are displayed in Table 1.

2.6. Western Blot Analysis. Protein lysates were harvested using a protein extraction reagent (Kangchen, China), and then, the protein concentration was determined using a BCA Protein Assay. Equal amounts of protein were separated on 10% or 15% SDS-polyacrylamide gel electrophoresis (PAGE) gels and transferred to polyvinylidene difluoride (PVDF, Pall, USA) membranes, and then, the membranes were blocked with 5% nonfat milk for 1 h. After that, the membranes were incubated with primary antibodies against p-AKT, AKT, ERK, p-ERK (dilution rate: 1 : 1000; all antibodies related to PI3K/AKT signaling or Erk1/2 signaling were bought from Cell Signaling Technology, Inc.), PDGF-BB (1 : 1000; Abcam, ab23914), Col-I (1 : 1000; Abcam, ab34710), OPN (1 : 1000; Abcam, ab8448), OCN (1 : 500; Abcam, ab93876), PPARγ2 (1 : 500; Abcam, ab209350), and β-actin (1 : 3000; Sigma). Then, the membranes were incubated with HRP-conjugated secondary antibodies (Sigma). Finally, the immunoblots were visualized using ECL Plus reagents (Amersham Pharmacia Biotech, USA) [23].

2.7. Human Umbilical Vein Endothelial Cell (HUVEC) Migration and Angiogenesis Assay. HUVECs were purchased from AllCells, Ltd. (Shanghai, China). HUVECs were cultured in endothelial basal medium (EBM, AllCells) devoid of growth factors [19]. To investigate the stimulation effects of PDGF-BB secreted by PDGF-B-modified BMSCs on HUVEC migration and angiogenesis, PDGF-B-modified BMSCs were cultured in six-well plates in DMEM (10^6 cells per 2 mL per well) for 24 h, and then, supernatants were collected for the following studies.

A transwell chemotactic migration model was used to examine the migration activity of HUVECs cultured in the supernatant from each group. HUVECs were seeded into the upper chambers of 24-well plates (10^4 cells per well) containing membranes with 8 μm pores (Corning Inc., Corning, NY). In the lower chambers, different media were added as follows: (a) supernatant from the Lenti-LacZ group, (b) supernatant from the Lenti-PDGF group supplemented with PD98059 (10 μM), (c) supernatant from the Lenti-PDGF group supplemented with LY294002 (10 μM), or (d) supernatant from the Lenti-PDGF group. After incubation for 12 h at 37°C, the migrated cells were fixed with 4% paraformaldehyde and stained with hematoxylin for 15 min at room temperature, and then, the cells that had migrated toward the lower side of the filter were observed using a fluorescence stereomicroscope (Leica, Germany). The number of migrated cells in each group was counted in 6 random fields per chamber.

To investigate whether phosphatidylinositol 3 kinase (PI3K)/AKT pathway and ERK1/2 signaling pathways were involved in PDGF-BB-mediated HUVEC migration and angiogenesis *in vitro*, HUVECs were preincubated with PD98059 (10 μM) or LY294002 (10 μM, PI3K/AKT inhibitor, Cell Signaling Technology) for 30 min, and then, the cells were incubated with the supernatants for 15 min. Protein lysates were harvested for Western blot analysis.

For the *in vitro* angiogenesis assay, HUVECs (3×10^4 cells/well) were seeded into 96-well culture plates, which were coated with Matrigel (BD Biosciences), and cultured with the following media: (a) supernatant from the Lenti-LacZ group, (b) supernatant from the Lenti-PDGF group supplemented with PD98059 (10 μM), (c) supernatant from the Lenti-PDGF group supplemented with LY294002 (10 μM), or (d) supernatant from the Lenti-PDGF group. After being cultured for 12 h, the cells were observed using an inverted light microscope (Leica, Germany). Five random

microscopic fields were photographed in each group, and then, the mesh numbers in each field were quantified using the angiogenesis analyzer of ImageJ.

2.8. Preparation of the BMSC/CPC Complex. Porous calcium phosphate cement (CPC) scaffolds (Rebone, China) were sterilized before use. BMSCs from each group were collected and resuspended in FBS-free medium, and then, a cell suspension (2×10^7 cells/mL) from each group was added to CPC scaffolds until saturated. A portion of these implants was used for *in vivo* animal studies, and the remainder was cultured for 1 or 3 days for scanning electron microscopy examination to observe BMSC spreading, adhesion, and proliferation on the CPC scaffold. After being cultured for 1 or 3 days *in vitro*, the samples were fixed in 2% glutaraldehyde, dehydrated in a series of graded ethanol solutions, sputter-coated with gold, and observed via scanning electron microscopy (SEM, Hitachi, Tokyo, Japan).

2.9. Animal Experiments. All procedures were approved by the Animal Research Committee of the Ninth People's Hospital, Shanghai Jiao Tong University School of Medicine. All surgical procedures were performed as described previously [22, 24]. Ten-week-old male F344 rats were used in this study. Briefly, the animals were anaesthetized by intraperitoneal injection of pentobarbital, and then, a 1.5 cm sagittal incision was made on the scalp to expose the calvarium. Two 5 mm diameter critical-sized defects were created using a trephine bur. A total of 24 rats were randomly divided into four groups to receive one of the following implants: (1) CPC ($n = 6$), (2) CPC with BMSCs ($n = 6$), (3) CPC with BMSCs/Lenti-LacZ ($n = 6$), or (4) CPC with BMSCs/Lenti-PDGF ($n = 6$).

2.10. Microfil Perfusion. Microfil (Flowtech, Carver, MA, USA) perfusion was used to identify blood vessel formation as previously described [25]. Briefly, the hair on the chest was shaved, and then, a long incision was made in the chest and abdomen (from the front limbs to the xiphoid process). The sternum was cut using scissors, and the rib cage was retracted laterally. The left ventricle was penetrated with an angiocatheter after the descending aorta was clamped. After the inferior vena cava was incised, 20 mL of heparinized saline was perfused, and then, 20 mL of Microfil was perfused at 2 mL/min, followed by perfusion with saline.

2.11. Radiography and Micro-CT Analysis. At 8 weeks post-surgery, all the rats in each group were sacrificed with an intraperitoneal overdose injection of pentobarbital. The calvarial bones were fixed in 10% formalin solution, and X-ray images of the skulls were obtained with a dental X-ray machine (Trophy, France). The morphology of the reconstructed skulls was evaluated using a micro-CT system (mCT-80, Scanco Medical, Switzerland) as previously described [26]. Briefly, the calvarial bone was scanned in high-resolution scanning mode (pixel matrix, 1024×1024; voxel size, 20 μm; slice thickness, 20 μm) to measure the bone volume. After scanning, three-dimensional images were reconstructed with GEHC Micro View software. Both the parameters bone mineral density (BMD) and the percentage of new bone volume relative to tissue volume were measured using auxiliary software (Scanco Medical AG, Switzerland).

2.12. Histological Analyses. After radiography and micro-CT analysis, the calvarial bones were dehydrated in ascending alcohol concentrations from 70% to 100%, and then, the samples were embedded in polymethylmethacrylate (PMMA). Sagittal sections of the central segment were cut using a microtome (Leica, Germany) and polished to a final thickness of approximately 40 μm. The sections were stained with Van Gieson's picro fuchsin to evaluate new bone formation. Red indicated new bone formation; residual CPC materials appeared black, and blue spots from the Microfil perfusion indicated blood perfusion. For hematoxylin and eosin (HE) staining, the calvarial bones were decalcified in 15% EDTA for 3 weeks and embedded with paraffin. A series of 5 mm sections were cut in the same manner as the hard tissue slices, and then, the sections were stained with HE for histological analysis. The area of newly formed bone (red area in both Van Gieson's picro fuchsin-stained sections and HE-stained sections) and blood vessels (blue spots indicated blood vessels filled with Microfil in the Van Gieson's picro fuchsin-stained sections; blood vessels were permeated with intraluminal red blood cells in the HE-stained sections) was quantitatively evaluated in four randomly selected sections from each group using Image pro 5.0 (Media Cybernetics, USA).

2.13. Statistical Analysis. The experimental data are presented as the mean ± standard derivation (SD). Differences between groups were analyzed via ANOVA with Tukey's post hoc test. Values of $P < 0.05$ were considered statistically significant.

3. Results

3.1. Gene Transduction and PDGF-BB Expression. Three days after gene transduction, inverted fluorescence microscopy observations and flow cytometry results showed that the transfection efficiency of the target gene PDGF-B was greater than 80% (Figure 1(a), Figure 1(b)). Both real-time RT-PCR and Western blotting results indicated that the expression of PDGF-BB in BMSCs was significantly upregulated after gene transduction in the Lenti-PDGF group (Figure 1(c), Figure 1(d)). ELISA results demonstrated that PDGF-B-modified BMSCs could stably and continuously secrete PDGF-BB at the protein level (Figure 1(e)).

3.2. Cell Differentiation Analysis. Osteogenic differentiation analysis showed that the expression of Col-I and OPN at both the mRNA and protein levels was increased in the Lenti-PDGF group compared with that in the Lenti-LacZ group at days 3 and 7 (Figure 2(a), Figure 2(b)). OCN was also remarkably increased at both the mRNA and protein levels at day 7 (Figure 2(a), Figure 2(b)). By contrast, there was no significant distinction between the Lenti-LacZ group and Lenti-PDGF group on day 3 (Figure 2(a), Figure 2(b)). ALP staining was more intense in the Lenti-PDGF group than in the Lenti-LacZ group, and the semiquantitative

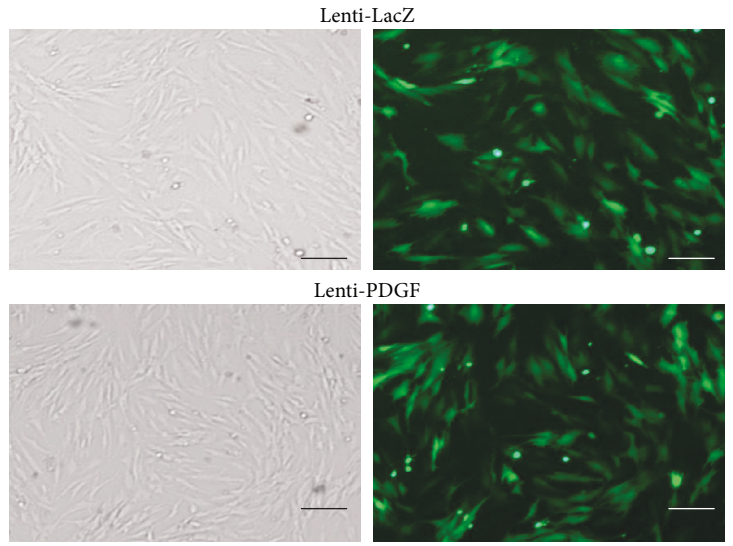

(a)

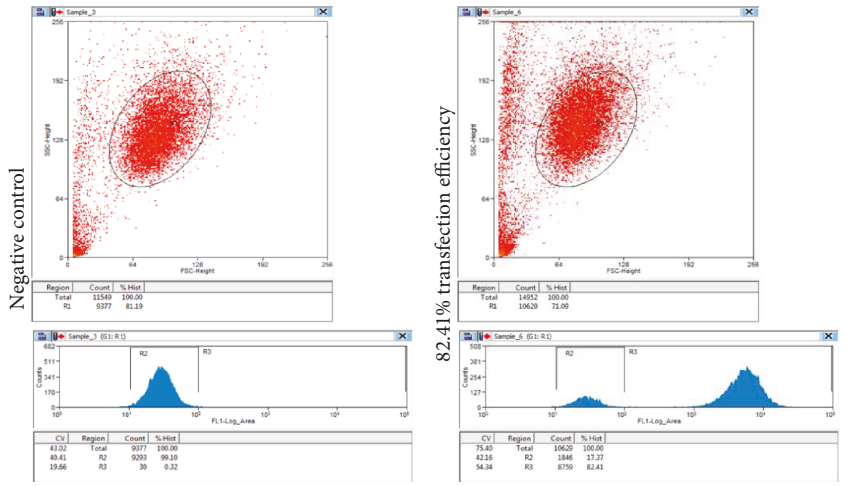

(b)

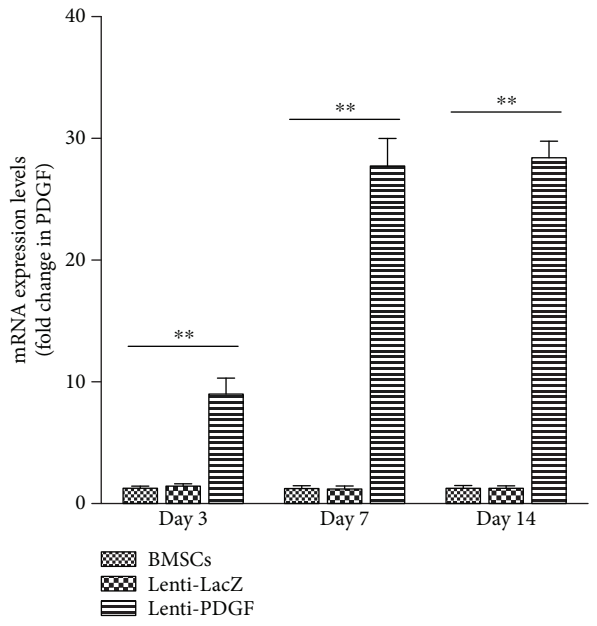

(c)

Figure 1: Continued.

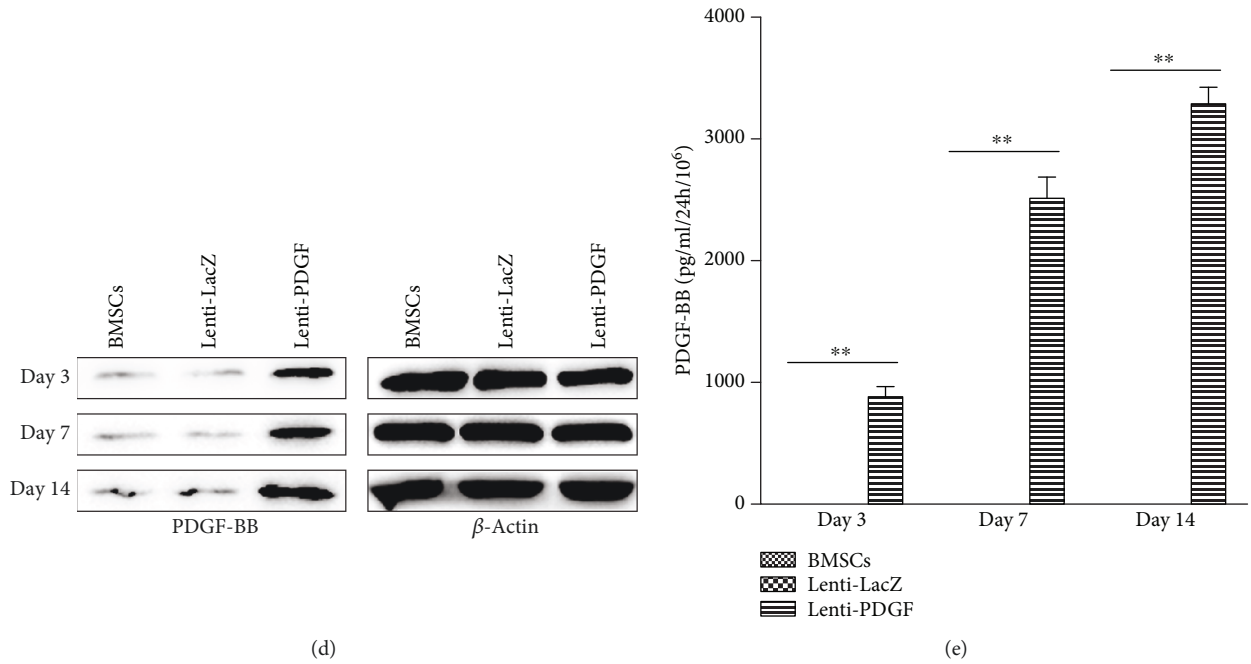

Figure 1: Detection of PDGF-BB expression. (a) At day 3 after gene transduction, both Lenti-LacZ-transfected and Lenti-PDGF-transfected BMSCs grew well and exhibited intense green fluorescence. (b) Flow cytometry assay showed 82.41% transfection efficiency. (c) *PDGF-B* mRNA expression in the BMSC, Lenti-LacZ, and Lenti-PDGF groups on days 3, 7, and 14. (d) PDGF-BB protein expression in the BMSC, Lenti-LacZ, and Lenti-PDGF groups on days 3, 7, and 14. (e) ELISA detection of PDGF-BB secretion *in vitro*. Scale bar: 100 μm; $^{**}P < 0.01$.

analysis showed a consistent result (Figure 2(c)). ARS staining revealed a significant increase in calcium deposition in the Lenti-PDGF group, and the quantitative analysis was consistent with the ARS staining results (Figure 2(d)).

Adipogenic differentiation analysis showed that lipid droplet accumulation was decreased significantly in the Lenti-PDGF group compared with that in the Lenti-LacZ group (Figure 3(a)). Oil Red O staining areas were remarkably decreased in the Lenti-PDGF group (Figure 3(b)). PPARγ2 mRNA and protein expression was significantly decreased in the Lenti-PDGF group compared with that in the Lenti-LacZ group (Figure 3(c), Figure 3(d)).

The ERK1/2 signaling pathway has been reported to be involved in mediating osteogenic and adipogenic differentiation of BMSCs [27, 28]. It is also known that PDGF-BB regulates the proliferation of several types of cells through the ERK1/2 signaling pathway [29, 30]. Therefore, we investigated whether this signaling pathway was activated in BMSCs by forcing PDGF-BB expression. Our results showed that the expression of phosphorylated ERK was significantly increased in PDGF-B-modified BMSCs (Figure 2(b)). The activation of the ERK1/2 signaling pathway was inhibited by administration of the inhibitor PD98059 (Figure 2(b)). The increased osteogenic differentiation and decreased adipogenic differentiation of BMSCs induced by PDGF-BB were also inhibited by administration of the inhibitor PD98059, which is an inhibitor of the ERK-MAPK signaling pathway (Figures 2 and 3). These results indicated that PDGF-BB enhances osteogenic differentiation and inhibits adipogenic differentiation of BMSCs via the ERK1/2 signaling pathway.

3.3. Effect of PDGF-BB on HUVEC Chemotactic Activity and Angiogenesis In Vitro. PDGF is a chemoattractant and has the ability to promote angiogenesis. Thus, PDGF has been widely used for tissue regeneration and repair. As shown in Figure 4(a), PDGF-BB secreted by PDGF-modified BMSCs strongly stimulated the migration of HUVECs. An approximately 2.5-fold stimulatory effect was observed in the supernatant from the Lenti-PDGF group compared with that from the Lenti-LacZ group (Figure 4(b)). The PI3K/AKT and ERK1/2 signaling pathways are involved in PDGF-induced migration in various cell types [31–35]. To further confirm whether PDGF-BB secreted by PDGF-B-modified BMSCs activates the intracellular pathway of HUVECs, the cells were pretreated with supernatant from the Lenti-PDGF group. The results showed that the expression of phosphorylated AKT and phosphorylated ERK was significantly increased, and their activation was inhibited by the corresponding inhibitor LY294002 or PD98059 (Figure 4(c)). In addition, the inhibitors significantly reduced the chemotactic effect of PDGF-BB secreted by PDGF-B-modified BMSCs on HUVECs (Figure 4(a), Figure 4(b)). *In vitro* angiogenesis analysis revealed that a significantly increased number of mesh formed by HUVEC structures were present in the Lenti-PDGF group compared with that in the Lenti-LacZ group after 12 h of culture (Figure 4(d), Figure 4(e)). The stimulatory effects were inhibited by the addition of the inhibitor LY294002 or inhibitor PD98059 (Figures 4(d) and 4(e)).

3.4. Cell Attachment and Viability on a CPC Scaffold. Cell attachment and growth of BMSCs seeded on porous CPC

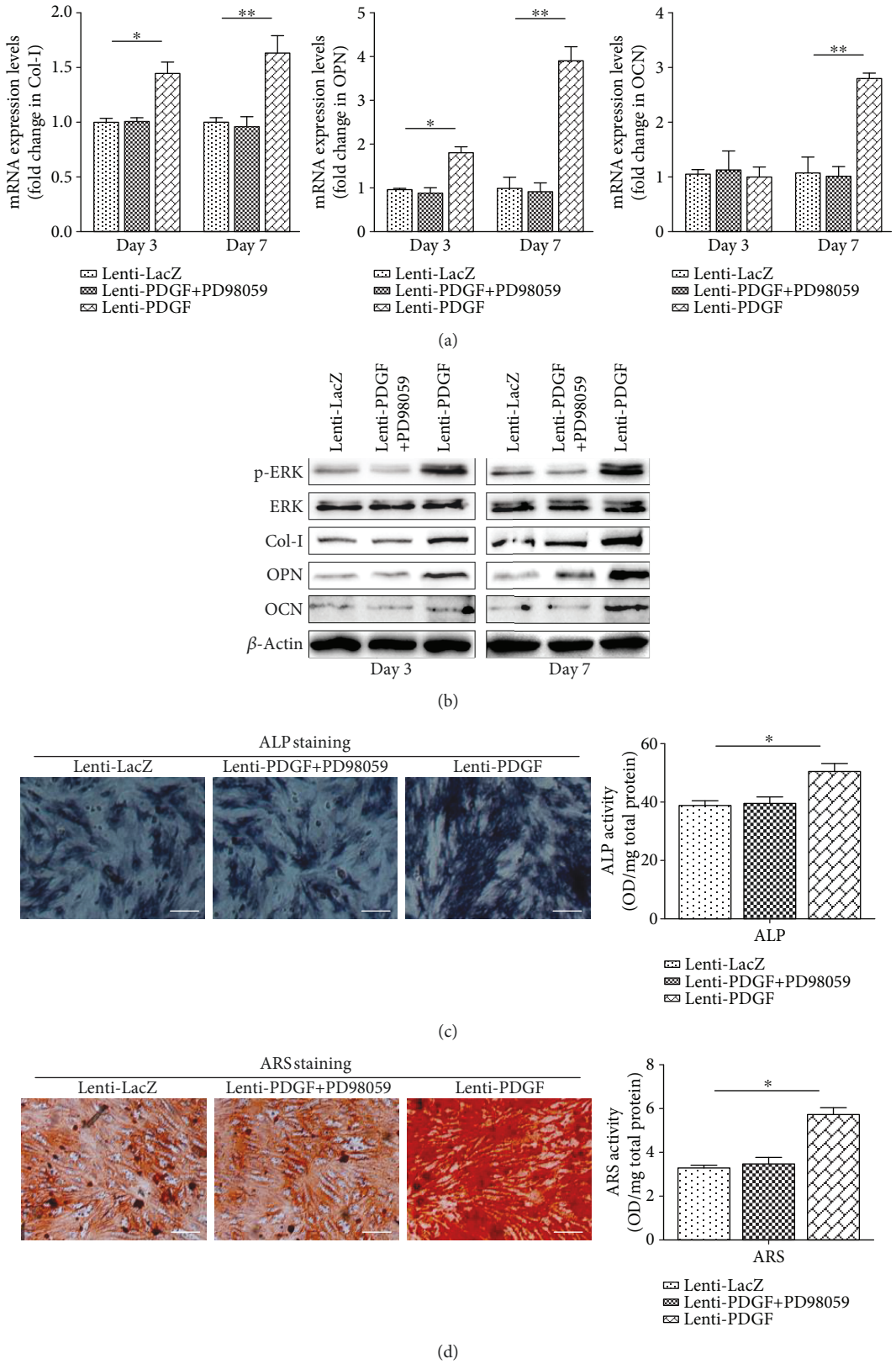

Figure 2: PDGF-BB enhanced BMSC osteogenic differentiation via ERK1/2 signaling pathways. (a) mRNA expression levels of *Col-I*, *OPN*, and *OCN* on days 3 and 7. (b) Protein expression levels of p-ERK, ERK, Col-I, OPN, and OCN on days 3 and 7. (c) ALP staining and semiquantitative analysis of ALP activity. (d) ARS staining and semiquantitative analysis of ARS staining. ALP: alkaline phosphatase; ARS: alizarin red S. Scale bar: 100 μm; $^{*}P < 0.05$; $^{**}P < 0.01$.

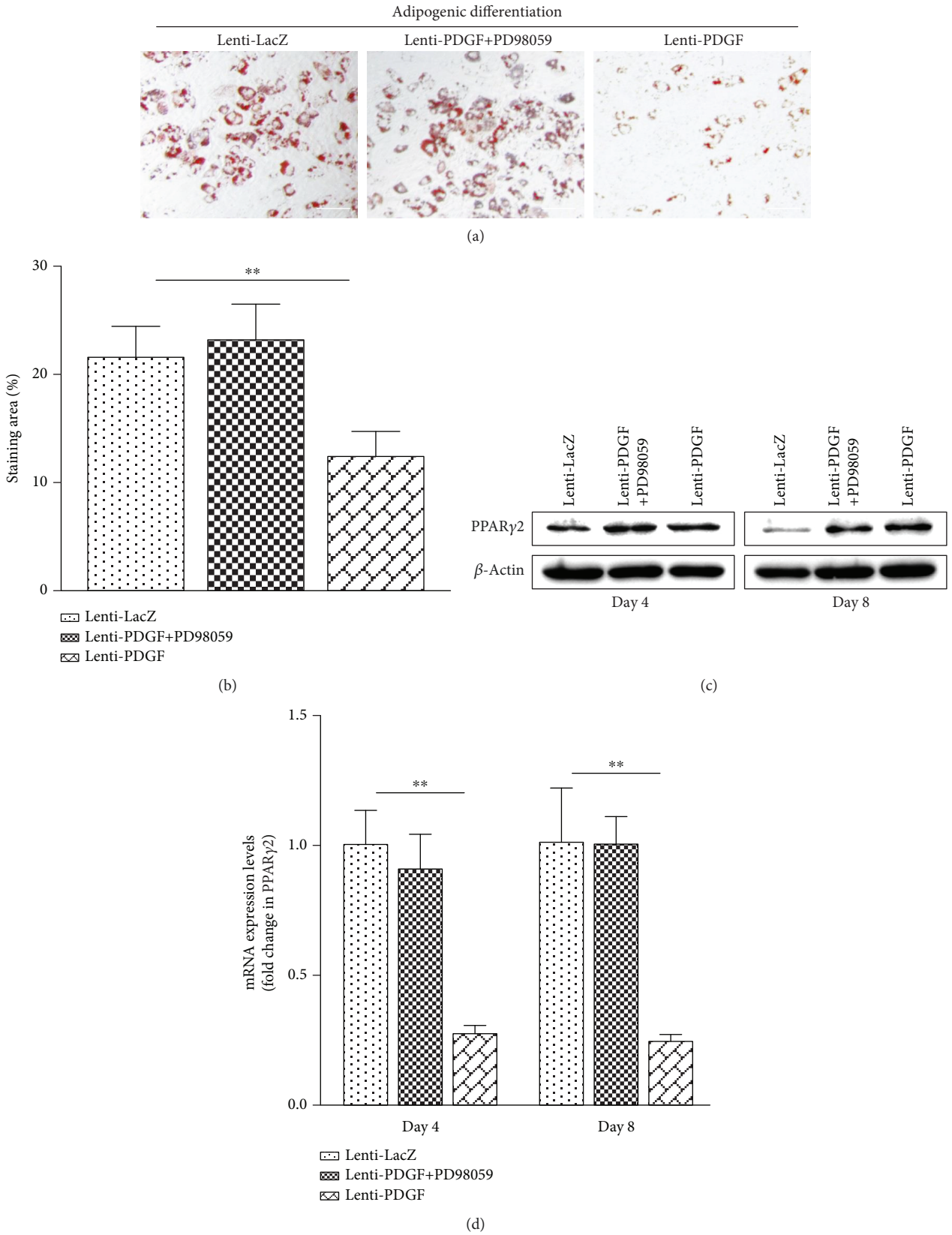

Figure 3: PDGF-BB inhibited BMSC adipogenic differentiation via ERK1/2 signaling pathways. (a) Oil Red O staining. (b) Oil Red O positively stained area in each group. (c) PPARγ2 protein expression. (d) *PPARγ2* mRNA expression. $^{**}P < 0.01$; scale bar: 100 μm.

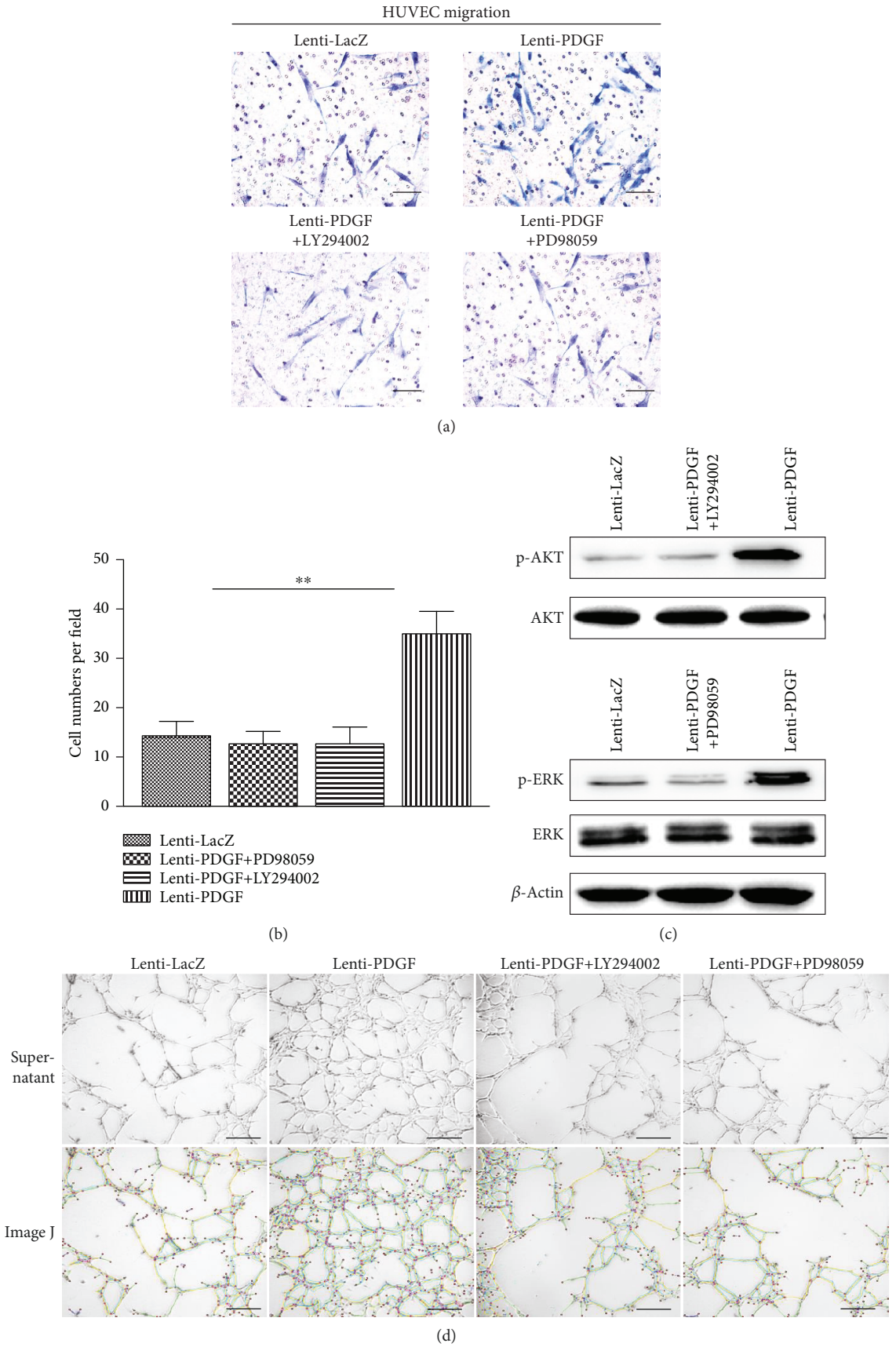

Figure 4: Continued.

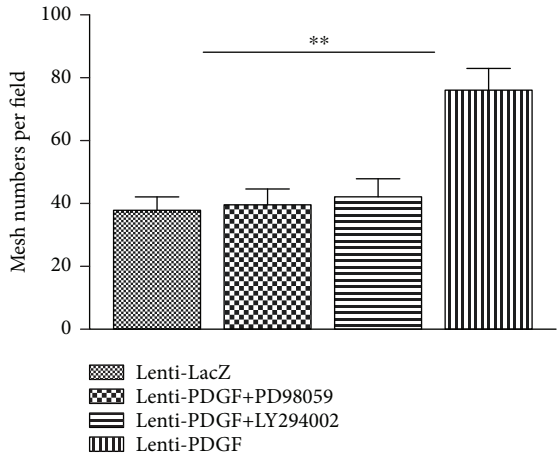

(e)

Figure 4: PDGF-BB secreted by Lenti-PDGF-B-modified BMSCs enhanced HUVEC migration and angiogenesis via the PI3K/AKT and ERK1/2 signaling pathways. (a) HUVECs on chemotaxis membranes stained with hematoxylin. (b) Cell numbers in each field. (c) PDGF-BB secreted by PDGF-B-modified-BMSCs induced ERK and AKT activation in HUVECs. (d) Optical images of HUVECs cultured on Matrigel with different supernatants after 12 h (upper panel); in the lower panel, ImageJ was used to measure the mesh number formed by HUVECs (green circle indicated mesh structure formed by HUVECs). (e) The mesh numbers in each group. $^{**}P < 0.01$; scale bar: 100 μm. HUVECs: human umbilical vein endothelial cells.

scaffolds were examined via SEM. As shown in Figure 5(a), CPC scaffolds showed an average pore diameter of 300–500 μm. After being cultured for 1 day *in vitro*, BMSCs attached and spread well on the surface of the CPC scaffolds. When cultured for 3 days *in vitro*, the cells grew well and formed cellular connections (Figure 5(b)). These results demonstrate that porous CPC scaffolds possess good biocompatibility, making them suitable for the following *in vivo* study. Figure 5(c) shows the surgical procedure employed for the *in vivo* transplantation.

3.5. Radiography and Micro-CT Measurement. X-ray images were taken at 8 weeks after explantation of the skull, and representative photographs of each group are shown in Figure 6(a). In the Lenti-PDGF group, the implants were closely integrated with the surrounding bone tissue and more radiopaque. In contrast, more radiotransparent areas were observed in the CPC group, BMSC group, and Lent-LacZ group. The morphology of newly formed bone was also reconstructed using micro-CT, and the three-dimensional (3D) reconstruction images of the skulls showed results consistent with the X-ray images (Figure 6(b)). From the transverse view, there was more newly formed bone tissue in the Lenti-PDGF group than in the CPC group, BMSC group, and Lenti-LacZ group (Figure 6(b)). Quantitative analysis showed that the BMD in the BMSC group (0.81 ± 0.04) and Lenti-LacZ group (0.80 ± 0.08) was higher than that in the CPC group (0.06 ± 0.57). The Lenti-PDGF group showed the highest BMD value (1.04 ± 0.13) among all the groups (Figure 6(c)). The BV/TV percentage in all groups (CPC, 7.00 ± 1.32; BMSCs, 16.00 ± 3.00; Lenti-LacZ, 15.67 ± 3.79; and Lenti-PDGF, 26.33 ± 3.51) was consistent with the BMD levels (Figure 6(d)).

3.6. Histological Analysis of Bone Regeneration. The undecalcified calvarial bone specimens from each group were stained with Van Gieson's picro fuchsin, and the decalcified specimens were stained for histological analysis. The results showed that newly formed bone tissue was present in all groups. However, the amount of newly formed bone tissue varied among the groups. More new bone tissue formation was observed in the Lenti-PDGF group than in the CPC, BMSC, and Lenti-LacZ groups, which was consistent with the radiography and micro-CT results (Figure 7(a)). Histomorphometric analysis showed that the percentage of new bone area was $6.33 \pm 1.52\%$ in the CPC group, $12.33 \pm 2.51\%$ in the BMSC group, $12.50 \pm 2.78\%$ in the Lenti-LacZ group, and $22.66 \pm 2.08\%$ in the Lenti-PDGF group (Figure 7(b)). These results indicate that PDGF-B-modified BMSCs significantly enhanced bone regeneration capacity in the calvarial bone defect model. To assess vascularization, Microfil perfusion was performed. As shown in Figure 7(a), each blue spot (green arrow) represents a blood vessel. HE staining also showed that the newly formed bone tissue was infiltrated with blood vessels (green arrow) with intraluminal red blood cells (Figure 7(a)). The area of newly formed blood vessels stained by Microfil perfusion was $0.66 \pm 0.15\%$ in the CPC group, $1.46 \pm 0.25\%$ in the BMSC group, $1.48 \pm 0.36\%$ in the Lenti-LacZ group, and $2.70 \pm 0.26\%$ in the Lenti-PDGF group (Figure 7(c)).

4. Discussion

In this study, we established a PDGF-B-modified BMSC line using a lentivirus vector to investigate the mechanism underlying PDGF-BB regulation of stem cell-based bone regeneration. Several studies have demonstrated that the ERK1/2

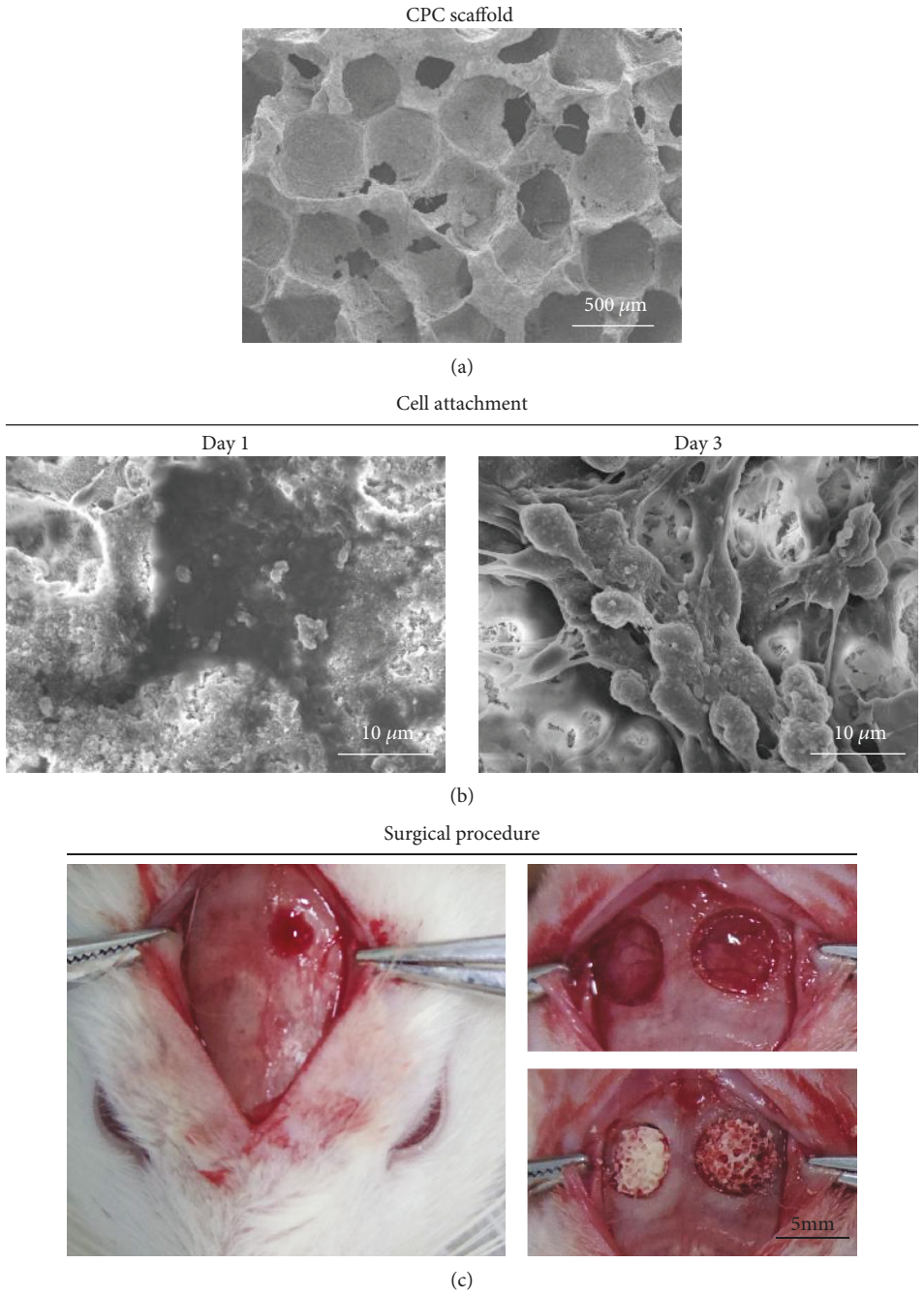

Figure 5: SEM analysis and surgical procedure. (a) SEM evaluation of porous CPC scaffold showing an average pore diameter of 300–500 μm. (b) BMSCs attached and spread well on CPC scaffolds. (c) Surgical procedure. CPC: calcium phosphate cement.

signaling pathway is involved in regulating osteogenic and adipogenic differentiation of MSCs [36]. Cell differentiation requires sustained activation of ERK, and transient activation of ERK leads to proliferation [37]. It is also known that PDGF-BB regulates the proliferation of several types of cells through the ERK1/2 signaling pathway [29, 30]. Thus, we speculated that continuous PDGF-BB expression may influence BMSC differentiation via the ERK signaling pathway. As we expected, forced expression of PDGF-BB in BMSCs activated the ERK signaling pathway, evidenced by the significantly increased expression of phosphorylated ERK in PDGF-B-modified BMSCs. Osteogenic-related markers, such as Col-I, OPN, and OCN, were upregulated by PDGF-BB. ALP activity and calcium deposition were also significantly increased by PDGF-BB overexpression. However, the enhanced osteogenic differentiation of PDGF-B-modified BMSCs was inhibited by the addition of PD98059, an inhibitor of the ERK-MAPK signaling pathway. It is well known that increased adipogenesis in the bone marrow decreases osteogenesis, which results in osteoporosis. The balance

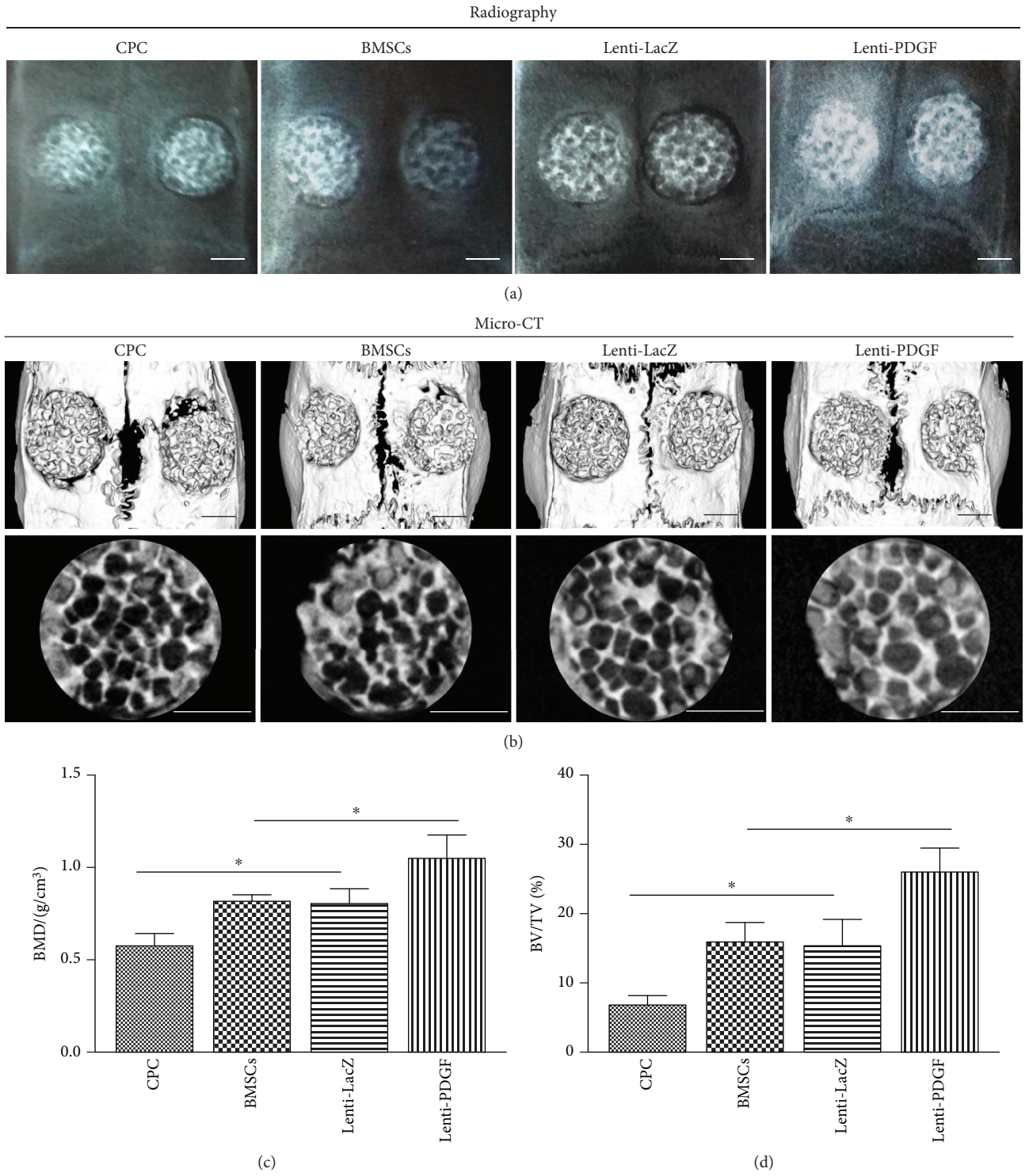

Figure 6: Radiography and micro-CT analysis. (a) Radiographic evaluation of the repaired skulls at 8 weeks. (b) 3D reconstruction images showing the reparative effect of the CPC, CPC with BMSCs, CPC with Lenti-LacZ-modified BMSCs, and CPC with PDGF-B-modified BMSCs. (c, d) Bone mineral density (BMD) and bone volume/total volume (BV/TV) analysis in each group. Scale bar: 2 mm; $^{*}P < 0.05$.

between osteogenic and adipogenic MSC differentiation is important for maintaining bone homeostasis [38]. Previous studies have demonstrated that PDGFRα signaling opposes adipogenesis of several types of cell [39, 40]. In this study, adipogenic differentiation of PDGF-B-modified BMSCs was also evaluated. Oil Red O staining area and lipid droplet accumulation were significantly decreased in PDGF-B-modified BMSCs. The expression of PPARγ2, a nuclear

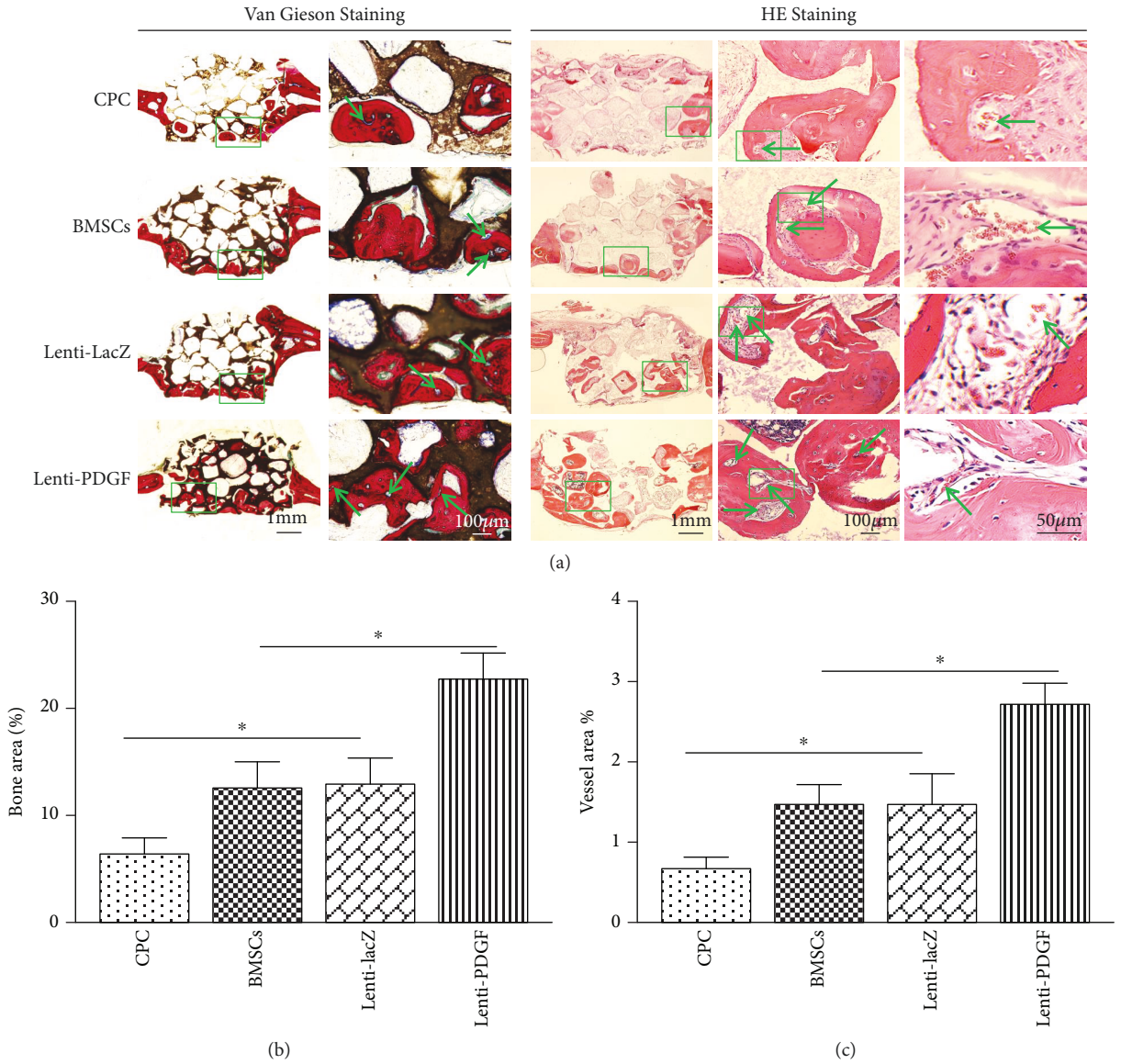

Figure 7: Histological analysis of newly formed bone and blood vessel in implants. (a) Histological images of each group. Left panel: Van Gieson staining, the new bone appears red, CPC appears black, and blue spots indicate blood vessels (green arrow); right panel: HE staining. The newly formed bone tissue was infiltrated with blood vessels (green arrow) with intraluminal red blood cells. (b) Histomorphometric analysis of the newly formed bone area. (c) Histomorphometric analysis of newly formed vessel area. $^{*}P < 0.05$.

receptor that can activate the expression of adipocyte phenotype-specific genes [41, 42], in PDGF-B-modified BMSCs was significantly decreased both at mRNA and protein levels. However, the inhibitory effect of PDGF-BB on BMSC adipogenic differentiation was inhibited by the addition of PD98059. Taken together, our results indicate that PDGF-BB can increase osteogenic differentiation while inhibiting adipogenic differentiation of BMSCs via ERK1/2 signaling pathways.

One of the key mechanisms by which stem cells promote tissue regeneration is secretion of soluble growth factors [43–46]. Previous studies have shown that PDGF-BB secreted by preosteoclasts induces vessel formation during bone modeling and remodeling [47]. After the lentiviral gene transduction, ELISA results showed that BMSCs stably and continuously secreted PDGF-BB. We further confirmed via HUVEC migration and angiogenesis assays that the secreted PDGF-BB protein possessed chemotactic activity and angiogenic activity. These results demonstrated that PDGF-BB secreted by PDGF-B-modified BMSCs stimulates the migration and angiogenic potential of HUVECs via the PI3K/AKT and ERK1/2 signaling pathways, which may further facilitate BMSC-based bone regeneration.

The effects of PDGF-BB on the regulation of BMSC-based bone regeneration *in vivo* were evaluated using a rat critical-sized calvarial defect model. Radiography and micro-CT measurements revealed that the implants were closely integrated with the surrounding bone tissue and more radiopaque in

the PDGF-BB overexpression group. According to the transverse view of the micro-CT, more newly formed bone tissue was present in the Lenti-PDGF group than in the other groups. Quantitative analysis showed that the BMD and BV/TV values were higher in the Lenti-PDGF group than those in the other groups. Histomorphometric analysis showed results consistent with the above findings, and the percentage of new bone area was significantly higher in the PDGF-BB-overexpressing group. Bone formation is driven by the presence of vasculature, and the formation of new vasculature, which transports oxygen, nutrients, and soluble factors, is necessary for new bone regeneration [25]. The area of newly formed blood vessels stained by Microfil perfusion was remarkably increased in the PDGF-BB-overexpressing group compared with that in the other groups. HE staining also showed that the newly formed bone tissue was infiltrated with blood vessels with intraluminal red blood cells. As described above, PDGF-BB is well known for its ability to promote angiogenesis, and it also plays an important role in maintaining the stabilization of newly formed blood vessels [11, 48, 49]. Thus, PDGF-BB secreted by PDGF-B-modified BMSCs would likely promote angiogenesis to facilitate bone regeneration.

5. Conclusions

In summary, our results demonstrated that overexpression of PDGF-BB in BMSCs increases osteogenic differentiation while inhibiting adipogenic differentiation via the ERK1/2 signaling pathway. PDGF-BB secreted by the PDGF-B-modified BMSCs significantly enhanced the migration and angiogenesis of vascular endothelial cells via the PI3K/AKT and ERK1/2 signaling pathways. The enhanced angiogenesis and osteogenesis capacity of BMSCs induced by PDGF-BB overexpression could promote *in vivo* vascularized bone regeneration. These findings indicate that PDGF-BB would be a powerful therapeutic regulator of angiogenesis and osteogenesis during bone formation and repair.

Data Availability

The data used to support the findings of this study are included within the article.

Conflicts of Interest

The authors indicated no potential conflicts of interest.

Authors' Contributions

Maolin Zhang and Wenwen Yu have contributed equally to this work.

Acknowledgments

This work was jointly supported by The National Key Research and Development Program of China (2016YFC1102900), the National Natural Science Foundation of China (81620108006).

References

[1] S. P. Bruder, A. A. Kurth, M. Shea, W. C. Hayes, N. Jaiswal, and S. Kadiyala, "Bone regeneration by implantation of purified, culture-expanded human mesenchymal stem cells," *Journal of Orthopaedic Research*, vol. 16, no. 2, pp. 155–162, 1998.

[2] X. Jiang, J. Zhao, S. Wang et al., "Mandibular repair in rats with premineralized silk scaffolds and BMP-2-modified bMSCs," *Biomaterials*, vol. 30, no. 27, pp. 4522–4532, 2009.

[3] H. Hou, X. Zhang, T. Tang, K. Dai, and R. Ge, "Enhancement of bone formation by genetically-engineered bone marrow stromal cells expressing BMP-2, VEGF and angiopoietin-1," *Biotechnology Letters*, vol. 31, no. 8, pp. 1183–1189, 2009.

[4] M. Tallquist and A. Kazlauskas, "PDGF signaling in cells and mice," *Cytokine & Growth Factor Reviews*, vol. 15, no. 4, pp. 205–213, 2004.

[5] R. M. Manzat Saplacan, L. Balacescu, C. Gherman et al., "The role of PDGFs and PDGFRs in colorectal cancer," *Mediators of Inflammation*, vol. 2017, 9 pages, 2017.

[6] L. Fredriksson, H. Li, and U. Eriksson, "The PDGF family: four gene products form five dimeric isoforms," *Cytokine & Growth Factor Reviews*, vol. 15, no. 4, pp. 197–204, 2004.

[7] R. Gruber, F. Karreth, F. Frommlet, M. B. Fischer, and G. Watzek, "Platelets are mitogenic for periosteum-derived cells," *Journal of Orthopaedic Research*, vol. 21, no. 5, pp. 941–948, 2003.

[8] M. H. Lee, B.-J. Kwon, M.-A. Koo, K. E. You, and J.-C. Park, "Mitogenesis of vascular smooth muscle cell stimulated by platelet-derived growth factor-bb is inhibited by blocking of intracellular signaling by epigallocatechin-3-O-gallate," *Oxidative Medicine and Cellular Longevity*, vol. 2013, Article ID 827905, 10 pages, 2013.

[9] Y. Ozaki, M. Nishimura, K. Sekiya et al., "Comprehensive analysis of chemotactic factors for bone marrow mesenchymal stem cells," *Stem Cells and Development*, vol. 16, no. 1, pp. 119–130, 2007.

[10] C. H. Heldin and B. Westermark, "Mechanism of action and in vivo role of platelet-derived growth factor," *Physiological Reviews*, vol. 79, no. 4, pp. 1283–1316, 1999.

[11] J. Homsi and A. I. Daud, "Spectrum of activity and mechanism of action of VEGF/PDGF inhibitors," *Cancer Control*, vol. 14, no. 3, pp. 285–294, 2007.

[12] M. C. Phipps, Y. Xu, and S. L. Bellis, "Delivery of platelet-derived growth factor as a chemotactic factor for mesenchymal stem cells by bone-mimetic electrospun scaffolds," *PLoS One*, vol. 7, no. 7, article e40831, 2012.

[13] A. I. Caplan and D. Correa, "PDGF in bone formation and regeneration: new insights into a novel mechanism involving MSCs," *Journal of Orthopaedic Research*, vol. 29, no. 12, pp. 1795–1803, 2011.

[14] L. Xu, W. Zhang, K. Lv, W. Yu, X. Jiang, and F. Zhang, "Peri-implant bone regeneration using rhPDGF-BB, BMSCs, and β-TCP in a canine model," *Clinical Implant Dentistry and Related Research*, vol. 18, no. 2, pp. 241–252, 2016.

[15] D. F. Bowen-Pope, T. W. Malpass, D. M. Foster, and R. Ross, "Platelet-derived growth factor in vivo: levels, activity, and rate of clearance," *Blood*, vol. 64, no. 2, pp. 458–469, 1984.

[16] C. Zhu, Q. Chang, D. Zou et al., "LvBMP-2 gene-modified BMSCs combined with calcium phosphate cement scaffolds for the repair of calvarial defects in rats," *Journal of Materials*

Science: Materials in Medicine, vol. 22, no. 8, pp. 1965–1973, 2011.

[17] W. Zhang, X. Zhang, S. Wang et al., "Comparison of the use of adipose tissue-derived and bone marrow-derived stem cells for rapid bone regeneration," *Journal of Dental Research*, vol. 92, no. 12, pp. 1136–1141, 2013.

[18] W. Zhang, C. Zhu, D. Ye et al., "Porous silk scaffolds for delivery of growth factors and stem cells to enhance bone regeneration," *PLoS One*, vol. 9, no. 7, article e102371, 2014.

[19] M. Zhang, F. Jiang, X. Zhang et al., "The effects of platelet-derived growth factor-BB on human dental pulp stem cells mediated dentin-pulp complex regeneration," *Stem Cells Translational Medicine*, vol. 6, no. 12, pp. 2126–2134, 2017.

[20] L. Xia, M. Zhang, Q. Chang et al., "Enhanced dentin-like mineralized tissue formation by AdShh-transfected human dental pulp cells and porous calcium phosphate cement," *PLoS One*, vol. 8, no. 5, article e62645, 2013.

[21] Y. Jin, W. Zhang, Y. Liu et al., "rhPDGF-BB via ERK pathway osteogenesis and adipogenesis balancing in ADSCs for critical-sized calvarial defect repair," *Tissue Engineering Part A*, vol. 20, no. 23-24, pp. 3303–3313, 2014.

[22] K. Lin, L. Xia, H. Li et al., "Enhanced osteoporotic bone regeneration by strontium-substituted calcium silicate bioactive ceramics," *Biomaterials*, vol. 34, no. 38, pp. 10028–10042, 2013.

[23] Y. Zhao, D. L. Zeng, L. G. Xia et al., "Osteogenic potential of bone marrow stromal cells derived from streptozotocin-induced diabetic rats," *International Journal of Molecular Medicine*, vol. 31, no. 3, pp. 614–620, 2013.

[24] D. Zou, Z. Zhang, D. Ye et al., "Repair of critical-sized rat calvarial defects using genetically engineered bone marrow-derived mesenchymal stem cells overexpressing hypoxia-inducible factor-1α," *Stem Cells*, vol. 29, no. 9, pp. 1380–1390, 2011.

[25] D. Zou, Z. Zhang, J. He et al., "Blood vessel formation in the tissue-engineered bone with the constitutively active form of HIF-1α mediated BMSCs," *Biomaterials*, vol. 33, no. 7, pp. 2097–2108, 2012.

[26] Y. Deng, H. Zhou, D. Zou et al., "The role of miR-31-modified adipose tissue-derived stem cells in repairing rat critical-sized calvarial defects," *Biomaterials*, vol. 34, no. 28, pp. 6717–6728, 2013.

[27] L. Fu, T. Tang, Y. Miao, S. Zhang, Z. Qu, and K. Dai, "Stimulation of osteogenic differentiation and inhibition of adipogenic differentiation in bone marrow stromal cells by alendronate via ERK and JNK activation," *Bone*, vol. 43, no. 1, pp. 40–47, 2008.

[28] Y. Zhao, S. Zhang, D. Zeng et al., "rhPDGF-BB promotes proliferation and osteogenic differentiation of bone marrow stromal cells from streptozotocin-induced diabetic rats through ERK pathway," *BioMed Research International*, vol. 2014, 9 pages, 2014.

[29] K. Kingsley, J. L. Huff, W. L. Rust et al., "ERK1/2 mediates PDGF-BB stimulated vascular smooth muscle cell proliferation and migration on laminin-5," *Biochemical and Biophysical Research*, vol. 293, no. 3, pp. 1000–1006, 2002.

[30] E. J. Battegay, J. Rupp, L. Iruela-Arispe, E. H. Sage, and M. Pech, "PDGF-BB modulates endothelial proliferation and angiogenesis in vitro via PDGF beta-receptors," *The Journal of Cell Biology*, vol. 125, no. 4, pp. 917–928, 1994.

[31] J. Fiedler, G. Röderer, K. P. Günther, and R. E. Brenner, "BMP-2, BMP-4, and PDGF-bb stimulate chemotactic migration of primary human mesenchymal progenitor cells," *Journal of Cellular Biochemistry*, vol. 87, no. 3, pp. 305–312, 2002.

[32] X. Sun, X. Gao, L. Zhou, L. Sun, and C. Lu, "PDGF-BB-induced MT1-MMP expression regulates proliferation and invasion of mesenchymal stem cells in 3-dimensional collagen via MEK/ERK1/2 and PI3K/AKT signaling," *Cellular Signalling*, vol. 25, no. 5, pp. 1279–1287, 2013.

[33] L. J. Yuan, C. C. Niu, S. S. Lin et al., "Additive effects of hyperbaric oxygen and platelet-derived growth factor-BB in chondrocyte transplantation via up-regulation expression of platelet-derived growth factor-beta receptor," *Journal of Orthopaedic Research*, vol. 27, no. 11, pp. 1439–1446, 2009.

[34] Y. J. Kang, E. S. Jeon, H. Y. Song et al., "Role of c-Jun N-terminal kinase in the PDGF-induced proliferation and migration of human adipose tissue-derived mesenchymal stem cells," *Journal of Cellular Biochemistry*, vol. 95, no. 6, pp. 1135–1145, 2005.

[35] D. Gentilini, M. Busacca, S. di Francesco, M. Vignali, P. Viganò, and A. M. di Blasio, "PI3K/Akt and ERK1/2 signalling pathways are involved in endometrial cell migration induced by 17β-estradiol and growth factors," *Molecular Human Reproduction*, vol. 13, no. 5, pp. 317–322, 2007.

[36] R. K. Jaiswal, N. Jaiswal, S. P. Bruder, G. Mbalaviele, D. R. Marshak, and M. F. Pittenger, "Adult human mesenchymal stem cell differentiation to the osteogenic or adipogenic lineage is regulated by mitogen-activated protein kinase," *The Journal of Biological Chemistry*, vol. 275, no. 13, pp. 9645–9652, 2000.

[37] C. J. Marshall, "Specificity of receptor tyrosine kinase signaling: transient versus sustained extracellular signal-regulated kinase activation," *Cell*, vol. 80, no. 2, pp. 179–185, 1995.

[38] J. Dragojevič, D. B. Logar, R. Komadina, and J. Marc, "Osteoblastogenesis and adipogenesis are higher in osteoarthritic than in osteoporotic bone tissue," *Archives of Medical Research*, vol. 42, no. 5, pp. 392–397, 2011.

[39] T. Iwayama, C. Steele, L. Yao et al., "PDGFRα signaling drives adipose tissue fibrosis by targeting progenitor cell plasticity," *Genes & Development*, vol. 29, no. 11, pp. 1106–1119, 2015.

[40] C. Sun, W. L. Berry, and L. E. Olson, "PDGFRα controls the balance of stromal and adipogenic cells during adipose tissue organogenesis," *Development*, vol. 144, no. 1, pp. 83–94, 2017.

[41] E. D. Rosen, P. Sarraf, A. E. Troy et al., "PPAR gamma is required for the differentiation of adipose tissue in vivo and in vitro," *Molecular Cell*, vol. 4, no. 4, pp. 611–617, 1999.

[42] Y. Barak, M. C. Nelson, E. S. Ong et al., "PPAR gamma is required for placental, cardiac, and adipose tissue development," *Molecular Cell*, vol. 4, no. 4, pp. 585–595, 1999.

[43] B. Parekkadan, D. van Poll, K. Suganuma et al., "Mesenchymal stem cell-derived molecules reverse fulminant hepatic failure," *PLoS One*, vol. 2, no. 9, article e941, 2007.

[44] A. I. Caplan and J. E. Dennis, "Mesenchymal stem cells as trophic mediators," *Journal of Cellular Biochemistry*, vol. 98, no. 5, pp. 1076–1084, 2006.

[45] S. Aggarwal and M. F. Pittenger, "Human mesenchymal stem cells modulate allogeneic immune cell responses," *Blood*, vol. 105, no. 4, pp. 1815–1822, 2005.

[46] T. Kinnaird, E. Stabile, M. S. Burnett et al., "Local delivery of marrow-derived stromal cells augments collateral perfusion through paracrine mechanisms," *Circulation*, vol. 109, no. 12, pp. 1543–1549, 2004.

[47] H. Xie, Z. Cui, L. Wang et al., "PDGF-BB secreted by preosteoclasts induces angiogenesis during coupling with osteogenesis," *Nature Medicine*, vol. 20, no. 11, pp. 1270–1278, 2014.

[48] G. D. Yancopoulos, S. Davis, N. W. Gale, J. S. Rudge, S. J. Wiegand, and J. Holash, "Vascular-specific growth factors and blood vessel formation," *Nature*, vol. 407, no. 6801, pp. 242–248, 2000.

[49] N. Ferrara, "VEGF and the quest for tumour angiogenesis factors," *Nature Reviews Cancer*, vol. 2, no. 10, pp. 795–803, 2002.